

# Detachment and sonoporation of adherent HeLa-cells by shock wave-induced cavitation

Claus-Dieter Ohl<sup>\*</sup>, Bernhard Wolfrum<sup>1</sup>

*TU Twente, Department of Applied Physics, Physics of Fluids, Postbus 217, 7500 AE Enschede, The Netherlands*

Received 27 March 2003; received in revised form 30 September 2003; accepted 14 October 2003

## Abstract

The interaction of lithotripter-generated shock waves with adherent cells is investigated using high-speed optical techniques. We show that shock waves permeabilize adherent cells *in vitro* through the action of cavitation bubbles. The bubbles are formed in the trailing tensile pulse of a lithotripter-generated shock wave where the pressure drops below the vapor pressure. Upon collapse of cavitation bubbles, a strong flow field is generated which accounts for two effects: first, detachment of cells from the substrate; and second, the temporary opening of cell membranes followed by molecular uptake, a process called sonoporation. Comparison of observed cell detachment with results from a theoretical model considering peeling cell detachment by a wall jet-induced shear stress shows reasonable agreement.

© 2003 Elsevier B.V. All rights reserved.

*Keywords:* Sonoporation; Drug delivery; Cell detachment; Shock wave; Cavitation

## 1. Introduction

Extracorporeal shock waves are widely used in well-established noninvasive local treatment methods such as renal stone fragmentation and bone healing [1]. However, tissue damage may occur as an undesired side effect during shock wave treatment [2–4]. New applications for lithotripters were proposed after it had been shown that shock waves could also enhance uptake of extracellular molecules into the cytoplasm of cells. In *in vitro* experiments, it was demonstrated that after shock wave application, some of the surviving cells had taken up non-membrane-permeant molecules [5]. Molecular uptake is a precondition for many biological and medical applications. For example, gene therapy requires the introduction of plasmids into the nucleus of host cells. Acoustic waves promise to be advantageous to certain drug delivery applications because they can be focused inside the patient's body without the need for surgery. Cell damage and the uptake of non-membrane-permeant molecules into cells following shock wave and ultrasound application have been investigated during the last years [6–8]. However, the exact mechanisms causing the

permeabilization of cell membranes allowing for drug delivery are not yet clarified. A large number of experiments using contrast agents to facilitate cavitation indicate that bubble activity plays a major role in transient and permanent membrane poration *in vivo* [9,10] and *in vitro* [11–13]. However, direct interactions of shock waves with membranes or membrane spanning proteins have also been suggested to be responsible for cell permeation [14,15]. Lokhandwalla and Sturtevant [16] describe the membrane rupture of red blood cells in suspension as an effect of shearing due to an extensional flow field caused either by radial bubble flow or by a non-uniform shock wave. In the present paper, we focus on adherent cells and show by microscopic high-speed optical techniques that cell detachment and molecular uptake is caused by the flow field induced from the collapse of cavitation bubbles. The resulting shear stress acting on the cells is estimated with an analytical solution for a wall jet fed by a constant flow [17] and used to predict the area of cell detachment with a peeling detachment model [18].

## 2. Materials and methods

### 2.1. Cell culture

HeLa cells were grown at 37 °C and 5% CO<sub>2</sub> in Iscove's modified Dulbecco's medium (Invitrogen, Breda Nether-

<sup>\*</sup> Corresponding author. Tel.: +31-53-489-5604; fax: +31-53-489-8068.

E-mail address: [c.d.ohl@tn.utwente.nl](mailto:c.d.ohl@tn.utwente.nl) (C.-D. Ohl).

<sup>1</sup> Permanent address: University of Göttingen, Third Physical Institute, Bürgerstr. 42-44, D-37073 Göttingen, Germany.

lands) supplemented with 10% fetal bovine serum (Invitrogen), antibiotics (100 units/ml penicillin, 100 µg/ml streptomycin), and 0.25 µg/ml amphotericin (Invitrogen). Cells were split with trypsin/EDTA (0.05%, Invitrogen) 1–3 days before use and plated in polystyrol culture flasks (25 cm<sup>2</sup> growth area, 60 ml volume, Nunc EasYFlask, TKT-120-170F, Fisher's Hertogenbosch, Netherlands). The cell doubling time was 48 h. The flasks were filled up with medium prior to shock wave exposure.

## 2.2. Viability stain

After shock wave exposure the suspension containing detached cells was removed carefully and subsequently centrifuged for 5 min at 1000 rpm (200 × g). The supernatant medium was removed and cells were resuspended in 1 ml PBS (Sigma, Zwijndrecht, Netherlands). Afterwards, cells were tested for viability using ethidium bromide/acridine orange (Fluka, Zwijndrecht, Netherlands) staining at final concentrations of 5 and 1.5 µg/ml, respectively. Ruptured cells appear orange due to the intercalation of ethidium bromide into their DNA and RNA. Cells with intact membranes are stained green by the membrane-permeant dye acridine orange. Dead and live cells were counted in a Neubauer chamber under a fluorescence microscope (Zeiss, Göttingen, Germany).

## 2.3. Transient membrane permeabilization

Transient membrane permeabilization was checked by the uptake of fluorescein isothiocyanate dextran (FITC-dextran, 20 kDa, FD-20S, Sigma) or calcein (1.02315.0005, Fisher's Hertogenbosch, Netherlands). We added non-membrane-permeant FITC-dextran (1 mg/ml) or calcein (1 mg/ml) to the cell medium before shock wave exposure. Dye uptake of attached cells was determined by fluorescence microscopy after washing the cells four times with PBS and adding ethidium bromide at a final concentration of 5 µg/ml. Transiently porated cells, loaded with FITC-dextran or calcein, appear green under fluorescence excitation. Permanently damaged cells appear orange due to ethidium bromide staining.

Detached cells were treated with the same procedure as described for viability staining. However, no acridine orange was used because it would not be possible to distinguish between living cells with or without FITC-dextran uptake.

## 2.4. Shock wave generation and microscopic observation

Shock waves were generated by a focused piezoceramic source, which was adapted from the commercial lithotripter Piezolith 3000 (Richard Wolf GmbH, Knittlingen, Germany). The lithotripter contains two piezoceramic layers with a diameter of 300 mm and a focusing angle of 94°. In our experiments, the operating voltage of the lithotripter was

set between 3.5 and 7 kV and only the frontal piezoceramic layer was used. The pressure in the free field at the lithotripter focus was measured with a calibrated needle type hydrophone of 1 mm diameter sensitive area consisting of a 20-µm-thick polyvinylidene fluoride (PVDF) foil (Dr. Pecha, University of Stuttgart, Germany). A typical recording at 6 kV is presented in Fig. 1. Due to the limited bandwidth of the hydrophone, the fast rise time cannot be resolved. Also the formation of cavitation bubbles at the hydrophone tip cause an underestimation of the duration of the negative pressure tail. However, the main features of the pressure wave are captured: the wave consists of a positive pressure pulse of about 1.5 µs with a steep front and an amplitude between 10 and 40 MPa (depending on the discharge voltage) followed by a tensile pressure pulse of amplitudes around 4 MPa, which lasts for several microseconds. The reproducibility of the waveform was high; the positive amplitude varied from shot-to-shot by less than 5%. Between consecutive shots at least 60 s were waited so that the bubbles generated had time to dissolve or float out of the focusing area.

A sketch of the experimental setup is presented in Fig. 2. The shock wave generator was oriented under an angle of 45° to the horizontal. The transducer was mounted in the bottom of a basin made of stainless steel with three glass windows. The basin was filled with approximately 50 l of degassed water having 3 mg O<sub>2</sub>/l.

The spatial position of the focus was first determined with the hydrophone and then marked by adjusting two beams from laser diodes, which crossed each other at the tip of the hydrophone.

For optical observations, we used a long-distance microscope (K2 with CF4 objective, Infinity, USA), which was

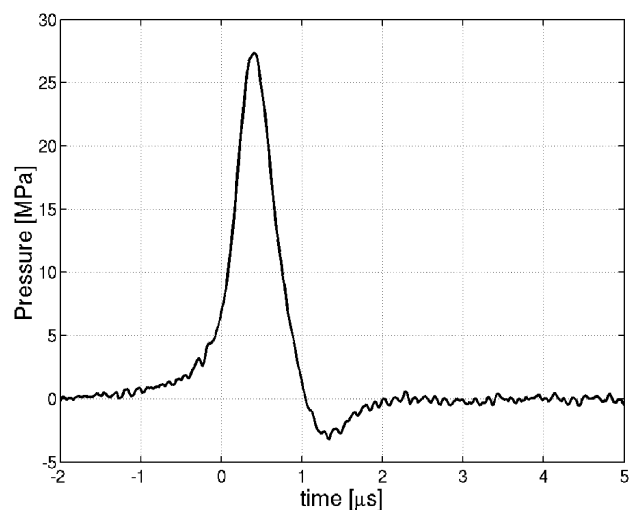


Fig. 1. A typical pressure recording of the shock wave passage at 6 kV discharge voltage on the piezoelectric layer of the lithotripter. The pressure rises to 28 MPa and drops after 1 µs to -3 MPa. Due to the limited rise time of the hydrophone, the rise time of the pressure amplitude is underestimated.

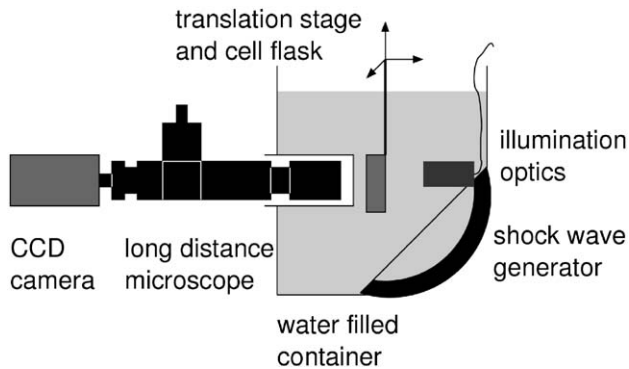


Fig. 2. A single shock wave is generated by a layer of piezoceramics and focused under an angle of  $45^\circ$  to the horizontal. The culture flask containing a monolayer of adherent HeLa cells is positioned with a three-axis micromanipulator. The dynamics is recorded with a double-frame camera (Imager 3S, LaVision) equipped with a long working distance microscope. Cells are illuminated with a strobe coupled into a fiber.

attached to a dual frame charged coupled device (CCD) camera (Imager 3S, LaVision, Göttingen, Germany). The camera is typically used for measuring particle displacements in particle image velocimetry (PIV) applications as it can record two separate stroboscopically illuminated frames in rapid succession. In the investigations presented here, this camera type was chosen because of its small pixel size combined with a high sensitivity and the ability to record fast events at moderate costs. The long-distance microscope was encased with cylindrical glass tube with the front side covered with a 5-mm-thick glass plate. Illumination was done by driving a pulsed light emitting diode (LED) with a home-built current amplifier. The system was triggered with a double pulse generator (HP 33120A, Agilent, Amstelveen, Netherlands). The setup ensured that the amplifier delivers between 1 and 3 Ampere only for a short duration and at very low duty cycles not to damage the semiconductor. Light from the diode was coupled into a 1 mm core polymethyl methacrylate (PMMA) fiber and brought to a two-lens system sealed and submerged into the water bath. The lenses collect and refocus the light while matching the numerical aperture to that of the long-distance microscope. The culture flask containing the cells was attached to a motorized three-axis translation stage (PI, Karlsruhe, Germany) with submicrometer resolution. Its position was controlled with a three-axis joystick.

In the data presented here, the flask was oriented with the cell substrate being first to be hit by the pressure pulse. However, we also conducted experiments with the bottom of the flask facing the camera, which yielded similar results.

The transmission coefficient of the substrate has been determined by comparing the peak positive amplitude of the shock wave,  $P^+$ , in the presence and absence of the substrate. A damping of 30% of the amplitude  $P^+$  is found with the substrate oriented at  $45^\circ$  to the direction of wave propagation and 10% for perpendicular orientation.

The temperature of the lithotripter bath and the cell medium was kept at approximately  $25^\circ\text{C}$ .

### 3. Results

#### 3.1. Cavitation inception on the substrate

First, the interaction of the shock wave on the bare substrate of the culture flask is investigated. Generally, in the trailing part of the shock wave, cavitation nuclei can grow due to the large tension of several megapascals of negative pressure. A growth of bubbles from these nuclei on the substrate in the absence of cells is presented in Fig. 3. The individual frames correspond to different times of a single experimental run. In the first frame of Fig. 3, the inner side of the polystyrol substrate is seen together with impurities related to the action of prior shock wave passages. We assume that the impurities are remnants of the locally disrupted substrate surface coating supporting the adhesion of cells. The substrate itself does not show cracks even after being subjected to 100 shock waves with the lithotripter working at 7 kV. The second frame in Fig. 3 is taken  $7\ \mu\text{s}$  after the shock wave passage. Here, the bubbles captured are blurred due to the relatively long exposure time of  $2\ \mu\text{s}$  and their explosive growth. In the third frame taken  $10\ \mu\text{s}$  later, the bubbles are already expanded to a size of around  $250\ \mu\text{m}$  in diameter. Shortly after frame 3, they expand to maximum size and collapses afterwards. The fourth frame of Fig. 3 displays the substrate 516 ms after shock wave passage. Remnants of the collapsed bubbles either dissolved or floated out of the field of view. Note that most of the impurities where cavitation was nucleated have disappeared. They might have been washed away by the strong flow generated during bubble collapse.

#### 3.2. Cell displacement and detachment

A typical example of the interaction of cavitation bubbles with cells is depicted in Fig. 4.

Time data is given with respect to the shock wave impact on the substrate. Shortly after that impact, we see two bubbles appearing due to the tensile pressure pulse following the shock wave. The distorted shape of the smaller bubble indicates that it is already in the collapse phase. Between the second and third frame of Fig. 4, both bubbles will develop a jet flow directed towards the substrate (rigid boundary), which subsequently results into an outward radial spreading flow. This flow pattern is sufficiently strong to detach cells located in the vicinity of the bubbles; see frames 3 and 4 in Fig. 4. There, cells only become detached at the positions where the bubble dynamics is visible.

Although most cells will detach a few microseconds after bubble collapse (frame 3), some cell movement and detachment can be detected at later times (frame 4).

The initial detachment of cells is directly correlated to the positions of cavitation bubbles. In cases where no bubble dynamics is observed, the cells remain in place. To document this finding, we present a high-speed sequence in Fig. 5

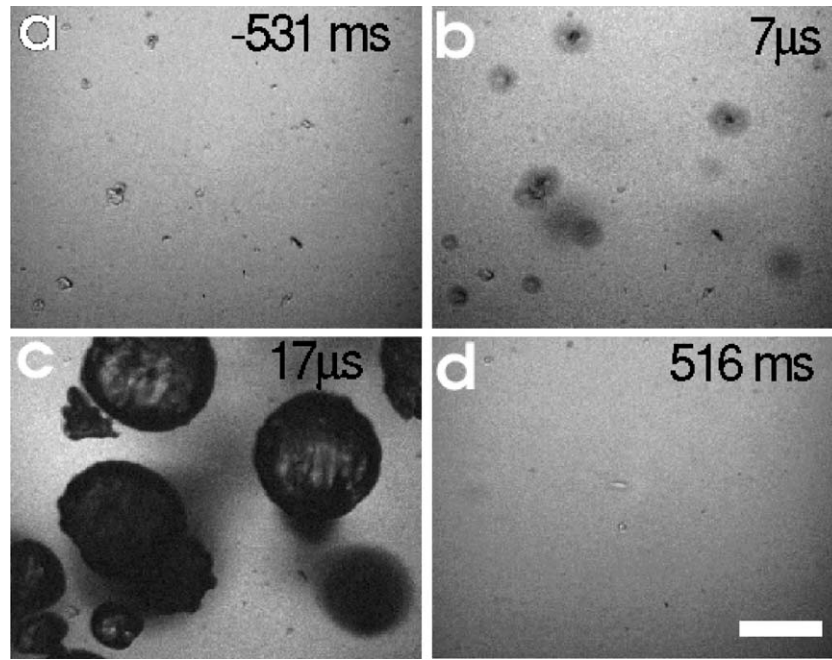


Fig. 3. Growth of cavitation bubbles on a culture flask after the impact of the shock wave at time  $t=0 \mu\text{s}$ . The first frame shows the substrate at the inner side of the flask with minor impurities presumably generated by prior interactions of shock waves with the substrate coating 531 ms before the shock wave is triggered. At  $t=7 \mu\text{s}$  cavitation inception on these impurities occurs. Large expanding bubbles are visible at  $17 \mu\text{s}$  and collapse approximately at  $t=200 \mu\text{s}$  (not shown here). At 516 ms after the shock wave impact, the substrate is partially cleared from the impurities indicating that the induced flow field from cavitation dynamics has flushed the prior nucleation sites. The individual frame width is 1 mm and the bar depicts 200  $\mu\text{m}$ .

where the cells are subjected to a shock wave of the same strength as in Fig. 4. However, in this case, no cavitation occurs in the field of view. By comparison of frame 1 (before the shock wave) and frame 4 (after the shock wave) of Fig. 5

no indications of either detachment or change in cell shape is seen. The absence of bubble activity suggests that no cavitation nuclei were present in the field of view during shock wave passage.

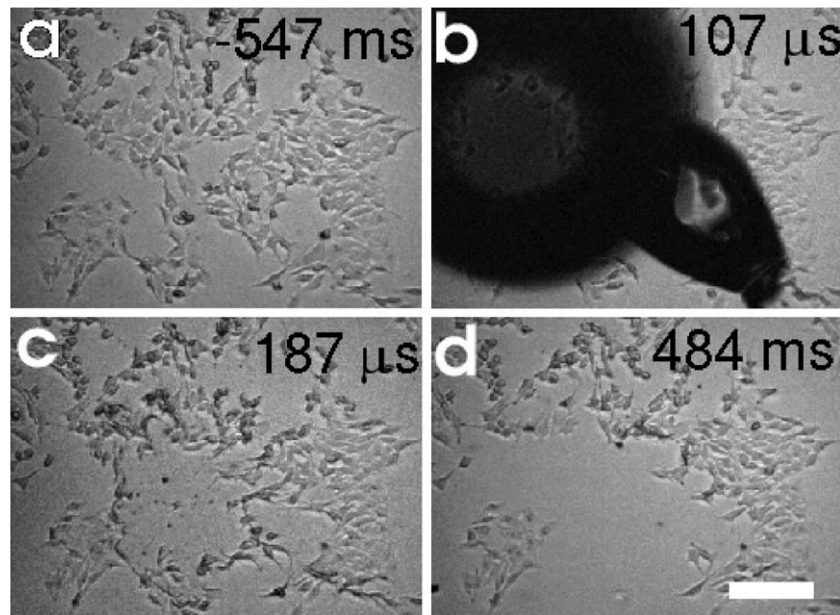


Fig. 4. Cavitation bubble nucleation on the substrate layer: picture sequence depicts exemplarily the detachment of cells following the shock wave passage. The lithotripter voltage was set to 6 kV. Time data in the upper left is given with respect to the shock front hitting the substrate. The first frame depicts the cells 547 ms before the shock wave hits the substrate. At  $t=107 \mu\text{s}$  (second frame), two bubbles are shown in their early collapse phase. Rapid detachment of cells can be seen 80  $\mu\text{s}$  later. After 484 ms, most of the cell detachment is completed, leaving a vacated region on the substrate (frame size  $0.96 \times 0.71 \text{ mm}$ , the bar depicts 200  $\mu\text{m}$ ).

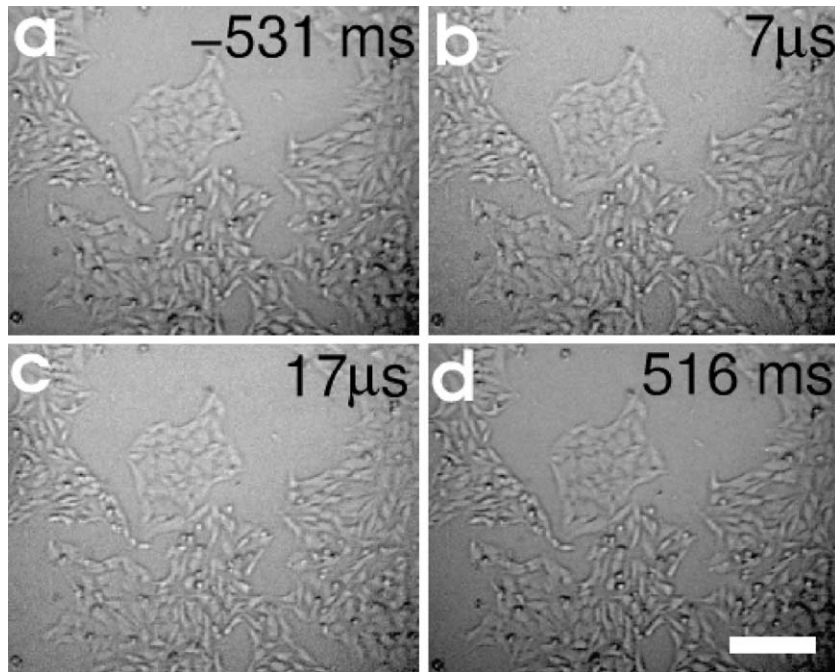


Fig. 5. An example sequence with no cavitation activity on the substrate: the timing of the individual frames 1–4 is given with respect to the impact of the shock wave on the substrate. The position and shape of the cells are unaffected by the passing shock wave (frame size  $0.96 \times 0.71$  mm, the bar depicts  $200 \mu\text{m}$ ).

### 3.3. Molecular uptake and cell viability

Fig. 6 depicts attached cells after shock wave exposure with the lithotripter operating at 6 kV. Prior to shock wave treatment, the cell medium was supplemented with FITC-dextran and treated as described above. It can be seen that the substrate is partially cleared of cells caused by cavitation

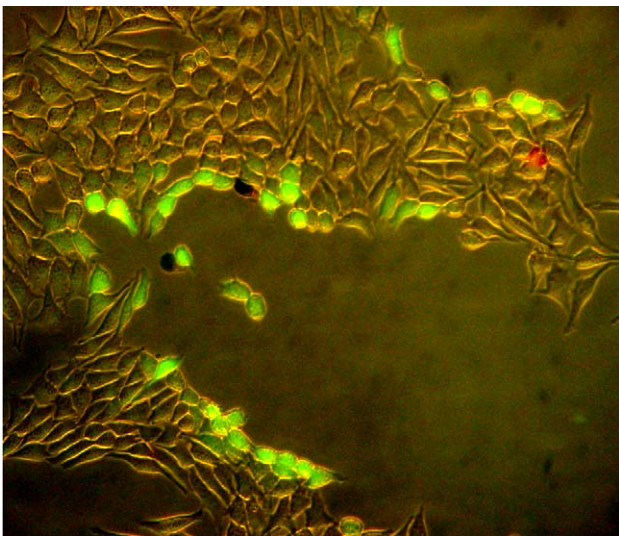


Fig. 6. The image shows cells after shock wave exposure and subsequent washing with PBS under a fluorescence microscope. Cells displaying green color have taken up FITC-dextran. Red color reveals dead cells because of the intercalation of ethidium bromide into the DNA (frame size  $0.72 \times 0.60$  mm).

activity. Cells, which have not been washed away but line the border between occupied and vacated regions, emit a strong green fluorescent light upon excitation originated by the uptake of FITC-dextran. Only slight emission of green fluorescence is detected for cells further away from the region of cavitation-induced detachment. Dead cells appear red or brown in the image due to the intercalation of ethidium bromide into the DNA of permanently damaged cells. Almost no dead cells can be seen in Fig. 6, which is reasonable since most of the destroyed cells will detach. Subsequently, they are swept away during washing with PBS.

The uptake of the smaller molecule calcein can be detected much further from the cavitation activity site than the uptake of FITC-dextran. The region of detected uptake of calcein spans  $4 \text{ mm}^2$  after one shot at 6 kV. The shape and size of the areas where detachment occurs are similar to those in the FITC-dextran experiments.

According to cell detachment, no uptake of either FITC-dextran or calcein could be detected when the strength of the shock waves were below cavitation threshold.

The molecular uptake and viability of detached cells was checked after multiple shock wave exposure with the lithotripter voltage set to 6 kV. Only one shot was taken at the same position and the flask was moved by 10 mm in the vertical or 2 mm in the horizontal position afterwards to detach cells from a large area. Overall, we counted 341 cells in three experiments carried out with the same setup. Almost 12% of the detached cells were permanently damaged and only 11% of the surviving cells had taken up FITC-dextran.

Culture growth of living cells after shock wave treatment has not been checked.

### 3.4. Model for shear flow-induced detachment

Generally, cavitation bubbles in the presence of a rigid boundary collapse with the formation of a jet flow in the direction to the boundary. This jet flow spreads out radially on the substrate where it is creating a boundary layer. We model the shear stress by considering that the wall jet is fed by a constant flow of constant thickness. Unfortunately, data for the velocity, duration and jet thickness are unavailable for the bubble radii of from 0.3 to 0.5 mm found in the experiments. Philipp and Lauterborn [19] experimentally found an impact velocity between 25 and 60 m/s for a bubble with 1.45 mm radius collapsing in contact with a boundary. On a longer time scale, when the bubble expands after the collapse, the velocity will decrease to considerable smaller values. We therefore assume an average jet velocity of 10 m/s acting for a duration of 50  $\mu$ s, which is in the order of the collapse time of a bubble with 0.5 mm radius. The diameter of the jet  $d$  is estimated to be in the order of a tenth of the bubble diameter, thus  $d = 100 \mu$ m. Using the above values, the Reynolds number,  $Re = dU_{jet}/\nu$ , with  $\nu = 10^{-6} \text{ m}^2/\text{s}$  being the kinematic viscosity of the liquid, becomes approximately  $Re = 1000$ , which suggests a mainly laminar flow.

The shear stress acting on the cells attached to the substrate surface,

$$\tau = \rho \nu \left( \frac{\partial u}{\partial y} \right)_{y=0}, \quad (1)$$

where  $\rho$  is the liquid density, is approximated with the analytical solution derived by Glauert [17]. There, a self-similar solution for the flow velocity has been derived,

which is strictly valid only for stationary laminar wall jets. The shear stress at the surface can be calculated by the definition Eq. (1):

$$\tau = \rho \left( \frac{125F^3}{216\nu x^{11}} \right)^{1/4}, \quad (2)$$

where the constant  $F$  is approximated

$$F = \frac{1}{16} U_{jet}^3 d^4 \quad (3)$$

for a flat velocity profile [17].

Fig. 7 (top) depicts the flow profile caused by a jet of 100  $\mu$ m in diameter and a velocity of 10 m/s for different distances from the impact region. The scale depicts a velocity of 10 m/s. In the bottom row of Fig. 7, the resulting shear stress is plotted, decreasing rapidly with a slope of  $-11/4$ , see Eq. (2).

To model the detachment of cells it is necessary to incorporate the duration the shear stress acts on the cells. Décavé et al. [18,20] have successfully modeled the process of detachment with a kinetic ansatz describing the breakage of the adhesive bonds between the cells and the substrate by a fracture process. They found that the number of detached cells per time unit (detachment rate  $k$ ) is related to the shear stress through Eq. (4)

$$k(\tau) = k_0 \frac{\exp(\tau/4\tau_0)}{\tau/4\tau_0}. \quad (4)$$

The two constants  $\tau_0$  and  $k_0$  in Eq. (4) are determined experimentally and depend mainly on surface and cell

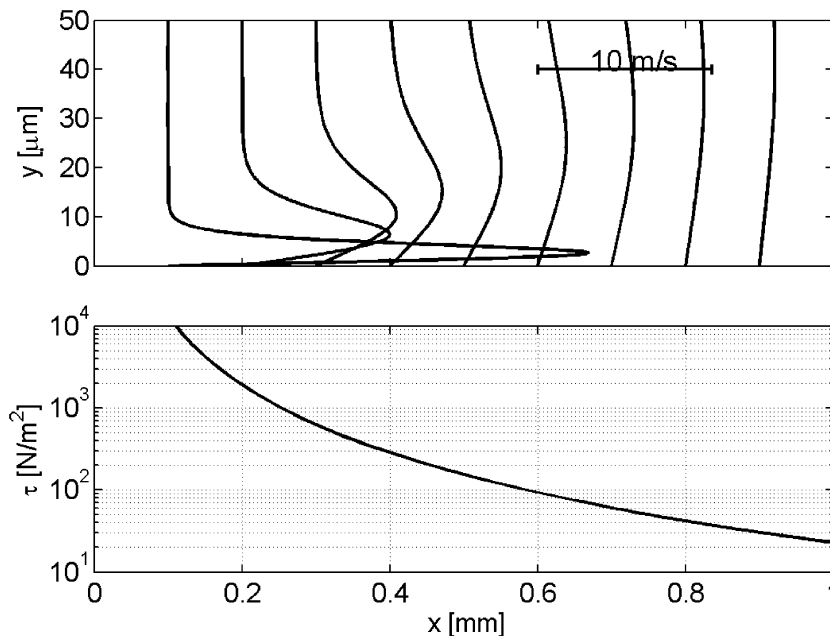


Fig. 7. In the upper plot, the flow profile of the wall jet as derived by Ref. [17] for a jet of 100  $\mu$ m in diameter impinging on the substrate at the origin with a velocity of 10 m/s is depicted. Below, the resulting shear stress as a function of the distance is plotted.

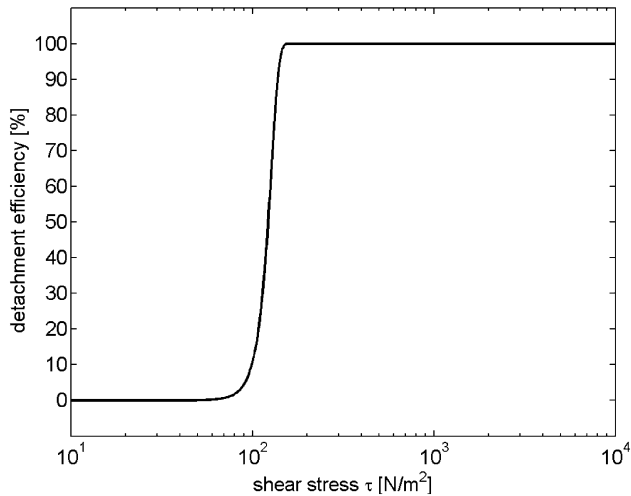


Fig. 8. The efficiency for detachment is plotted for a fluid loading of 50  $\mu$ s duration as a function of the applied shear stress. For shear stresses above 160 N/m<sup>2</sup>, 100% of the cells are detached (see text).

properties. As an approximation, we use  $\tau_0 = 0.08$  Pa and  $k_0 = 0.012/\text{min}$  as found in Ref. [18] for *Dictyostelium discoideum* cells on a glass substrate. The percentage of detached cells,  $n(\tau, t)$ , follows from the solution of a rate equation:

$$n(\tau, t) = 1 - \exp(-k(\tau)t). \quad (5)$$

With the assumptions that the fluid loading lasts for 50  $\mu$ s as described above, the percentage of detached cells can be obtained from Fig. 8. For shear stresses above 160 N/m<sup>2</sup>, full detachment is achieved. This compares with a circular detachment area of 0.5 mm in radius (Fig. 7) and is on the same order as our experimental results (typical radius  $r \approx 0.2$  mm). To achieve a better estimation of the shear stress and resulting detachment, turbulent jet-flow dynamics, bubble–bubble interactions as well as appropriate detachment parameters for the given cell and surface type should be taken into account.

#### 4. Discussion

From our experiments, we can conclude that the cell detachment is caused by the generation of cavitation. This statement is based on the fact that the detachment on cells was only observed when cavitation bubble dynamics took place. By comparing Figs. 4 and 5, it is found that the impact of the shock wave onto the substrate in the absence of cavitation does not contribute to cell detachment. Thus, more complex scenarios such as the generation of surface waves and shearing action by pressure gradients [16] can be neglected.

Cavitation bubbles incept at impurities during the tensile pressure pulse following the shock wave. In a simple model, we can separate the bubble dynamics in three phases: (1) first, we have an initial growth of the bubble after cavitation inception. The liquid surrounding the bubble will be forced

outward from the bubble center. At the rigid boundary of the substrate, the flow will be redirected resulting in an outward radial streaming along the substrate with its center located at the projection of the bubble center onto the substrate. (2) At the beginning of bubble collapse, the situation is reversed. Liquid flow will be directed toward the center of the bubble resulting in an inward streaming along the substrate. However, due to the drag of the flow caused by the rigid boundary, the bubble collapse will not be spherical. (3) Upon final collapse, the bubble will form a jet towards the substrate [19,21,22,23]. The aspherical collapse induces again an outward radial streaming along the substrate surface [23].

The bubble behavior becomes more complicated if bubble–bubble interactions are taken into account. During all phases of bubble activity, the cells on the substrate will be subjected to shear stress. However, it is probable that the jet-induced flow generates the dominant shear stress, which is sufficiently strong to break the adherent forces of the cells in its vicinity. As a result of this flow-induced detachment, a roughly circular vacated region appears on the substrate. Cells, which are not detached but line the border of vacated regions are subjected to stress caused by the flow field. The stress exerted on the cells will decrease with increasing distance to the bubble collapse center. Depending on the strength of the stress, membranes may be transiently ruptured facilitating the uptake of molecules.

We observed that in contrast to FITC-dextran, the uptake of calcein takes place at distances as far as 2 mm from the center of cell detachment. This indicates that even at large distance from the center of bubble activity some permeabilization of membranes is induced. However, either number or size of the pores induced by the weaker flow field is too small or their life span is too short to allow for detectable uptake of FITC-dextran. The rapid breaking of cell–cell adhesion bonds of those cells lining the border of vacated regions might also contribute to stronger perforation, enabling the uptake of larger molecules.

The molecular uptake of detached cells after multiple shock wave exposure is very low compared to attached cells lining the border of vacated regions after single shock wave application. One might expect that cells, which are detached, have been subjected to an even stronger shear stress and consequently, should either be transiently permeabilized or destroyed. However, it was shown that cell detachment could be facilitated by previous shock wave exposure in neighboring regions, which was probably caused by subsequent breaking of adhesion points between cells and the substrate near the cavitation activity site. Therefore, it might be possible that many detached cells have not been exposed to the threshold shear stress necessary to generate sufficient pores for molecular delivery.

It is also possible that the mechanical stimulus induces a reaction inside the cell, which will trigger the weakening of adhesion forces allowing for large-scale detachment [24].

An additional finding is that after application of two to five shock waves at constant amplitude, no further bubbles

could be nucleated at that specific site. Only, after increasing the charging voltage of the shock wave generator, or moving the substrate by several millimeters (the size of the focal diameter), the new bubbles were nucleated again. These findings support the hypothesis of cavitation inception from in some means stabilized microbubbles not visible within the resolution limit of the optical setup [25,26].

We have shown with high-speed optical techniques that cell detachment and molecular uptake of adherent HeLa cells after shock wave application is caused by activity of cavitation bubbles. Bubbles incept during the trailing tensile pressure pulse of the lithotripter shock wave. They generate a flow field, which induces shear stress on the adherent cells in its vicinity. The shear stress has been estimated using a wall jet model. It is sufficiently strong to break adhesion forces between cells and substrate, destroy cells, or transiently permeabilize cell membranes facilitating molecular uptake.

Comparison of observed cell detachment with results from a peeling detachment model show reasonable agreement. However, we cannot rule out that apart from the wall jet, further mechanisms contribute to the cell detachment, e.g. pressure fluctuations caused by the impacting liquid jet and by the so-called liquid splash [23].

## Acknowledgements

We are very thankful to Prof. D. Lohse for pointing us to Ref. [17]. He encouraged us to apply the self-similarity solution as done in Sect. 3.4 of this paper. We thank Prof. M. Delius who drew our attention with his investigation that a single shock wave can detach cultivated HeLa cells from a substrate. For help with the experimental part, we thank Roy Ikin and Manish Arora. One of the authors, B. Wolfrum, has received partial funding from NWO, and we thank Prof. W. Lauterborn and Prof. D. Lohse for their collaboration. Additionally, we would like to thank an anonymous referee for improving the manuscript. The work is supported by FOM 00PMT04.

## References

- [1] A.J. Coleman, J.E. Saunders, A review of the physical properties and biological effects of the high amplitude acoustic fields used in extracorporeal lithotripsy, *Ultrasonics* 31 (1993) 75–89.
- [2] M. Delius, R. Denk, C. Berding, H.-G. Liebich, M. Jordan, W. Brendel, Biological effects of shock waves: cavitation by shock waves in piglet liver, *Ultrasound Med. Biol.* 16 (1990) 467–472.
- [3] M. Delius, Medical applications and bioeffects of extracorporeal shock waves, *Shock Waves* 4 (1994) 55–72.
- [4] P. Zhong, X.F. Xi, S.L. Zhu, F.H. Cocks, G.M. Preminger, Recent developments in SWL physics research, *J. Endourol.* 13 (1999) 611–617.
- [5] M. Delius, P.-H. Hofschneider, U. Lauer, K. Messmer, Extracorporeal shock waves for gene therapy? *Lancet* 345 (1995) 1377.
- [6] P.E. Huber, J. Jenne, J. Debus, M.F. Wannemacher, P. Pfisterer, A comparison of shock wave and sinusoidal-focused ultrasound-induced localized transfection of HeLa cells, *Ultrasound Med. Biol.* 25 (1999) 1451–1457.
- [7] T. Kodama, M.R. Hamblin, A.G. Doukas, Cytoplasmic molecular delivery with shock waves: importance of impulse, *Biophys. J.* 79 (2000) 1821–1832.
- [8] K. Tschoep, G. Hartmann, R. Jox, S. Thompson, A. Eigler, A. Krug, S. Erhardt, G. Adams, S. Endres, M. Delius, Shock waves: a novel method for cytoplasmic delivery of antisense oligonucleotides, *J. Mol. Med.* 79 (2001) 306–313.
- [9] D. Dalecki, S.Z. Child, C.H. Raeman, C. Xing, S. Gracewski, E.L. Carstensen, Bioeffects of positive and negative acoustic pressures in mice infused with microbubbles, *Ultrasound Med. Biol.* 26 (2000) 1327–1332.
- [10] D.L. Miller, J. Quddus, Diagnostic ultrasound activation of contrast agent gas bodies induces capillary rupture in mice, *Proc. Natl. Acad. Sci.* 97 (2000) 10179–10184.
- [11] S. Bao, B.D. Thrall, D.L. Miller, Transfection of a reporter plasmid into cultured cells by sonoporation in vitro, *Ultrasound Med. Biol.* 23 (1997) 953–959.
- [12] M. Ward, J. Wu, J.-F. Chiu, Ultrasound-induced cell lysis and sonoporation enhanced by contrast agents, *J. Acoust. Soc. Am.* 105 (1999) 2951–2957.
- [13] H.R. Guzmán, D.X. Nguyen, S. Khan, M.R. Prausnitz, Ultrasound-mediated disruption of cell membranes: I. Quantification of molecular uptake and cell viability, *J. Acoust. Soc. Am.* 110 (2001) 588–596.
- [14] A.G. Doukas, D.J. McAuliffe, S. Lee, V. Venugopalan, T.J. Flotte, Physical factors involved in stress-wave-induced cell injury: the effects of stress gradient, *Ultrasound Med. Biol.* 21 (1995) 961–967.
- [15] S. Lee, D.J. McAuliffe, H. Zhang, Z. Xu, J. Taitelbaum, T.J. Flotte, A.G. Doukas, Stress-wave-induced membrane permeation of red blood cells is facilitated by aquaporins, *Ultrasound Med. Biol.* 23 (1997) 1089–1094.
- [16] M. Lokhandwalla, B. Sturtevant, Mechanical haemolysis in shock wave lithotripsy (SWL): I. Analysis of cell deformation due to SWL flow-fields, *Phys. Med. Biol.* 46 (2001) 413–437.
- [17] M.B. Glauert, The wall jet, *J. Fluid Mech.* 1 (1956) 625–643.
- [18] E. Décavé, D. Garrivier, Y. Bréchet, B. Fourcade, F. Bruckert, Shear flow-induced detachment kinetics of *Dictyostelium discoideum* cells from solid substrate, *Biophys. J.* 82 (2002) 2382–2395.
- [19] A. Philipp, W. Lauterborn, Cavitation erosion by single laser-produced bubbles, *J. Fluid Mech.* 361 (1998) 75–116.
- [20] E. Décavé, D. Garrivier, Y. Bréchet, F. Bruckert, B. Fourcade, Peeling process in living cell movement under shear flow, *Phys. Rev. Lett.* 89 (2002) 1081011–1081014.
- [21] W. Lauterborn, H. Bolle, Experimental investigations of cavitation-bubble collapse in the neighborhood of a solid boundary, *J. Fluid Mech.* 72 (1975) 391–399.
- [22] J.R. Blake, M.R. Hooton, P.B. Robinson, R.P. Tong, Collapsing cavities, toroidal bubbles and jet impact, *Phil. Trans. Roy. Soc. Lond. A* 355 (1997) 537–550.
- [23] E.A. Brujan, G.S. Keen, A. Vogel, J.R. Blake, The final stage of the collapse of a cavitation bubble close to a rigid boundary, *Phys. Fluids* 14 (2002) 85–92.
- [24] C. Zhu, G. Bao, N. Wang, Cell mechanics: mechanical response, cell adhesion, and molecular deformation, *Annu. Rev. Biomed. Eng.* 2 (2000) 189–226.
- [25] C.-D. Ohl, Cavitation inception following shock wave passage, *Phys. Fluids* 14 (2002) 3512–3521.
- [26] O.A. Sapozhnikov, V.A. Khokhlova, M.R. Bailey, J.C. Williams, J.A. McAteer, R.O. Cleveland, L.A. Crum, Effect of overpressure and pulse repetition frequency on cavitation in shock wave lithotripsy, *J. Acoust. Soc. Am.* 112 (2002) 1183–1195.